Combinatorial Screening of Bimetallic Electrocatalysts for Nitrogen Reduction to Ammonia Using a High-Throughput Gas Diffusion Electrode Cell Design

Kolen, Martin; Antoniadis, Grigorios; Schreuders, Herman; Boshuizen, Bart; van Noordenne, Dylan D.; Ripepi, Davide; Smith, Wilson A.; Mulder, Fokko M.

DOI
10.1149/1945-7111/aca6a7

Publication date
2022

Document Version
Final published version

Published in
Journal of the Electrochemical Society

Journal of The Electrochemical Society

Combinatorial Screening of Bimetallic Electrocatalysts for Nitrogen Reduction to Ammonia Using a High-Throughput Gas Diffusion Electrode Cell Design

Journal of The Electrochemical Society, 2022 **169** 124506

Combinatorial Screening of Bimetallic Electrocatalysts for Nitrogen Reduction to Ammonia Using a High-Throughput Gas Diffusion Electrode Cell Design

Martin Kolen,[z] Grigorios Antoniadis, Herman Schreuders, Bart Boshuizen, Dylan D. van Noordenne, Davide Ripepi, Wilson A. Smith, and Fokko M. Mulder[z]

Materials for Energy Conversion and Storage (MECS), Department of Chemical Engineering, Faculty of Applied Sciences, Delft University of Technology, van der Maasweg 9, 2629 HZ Delft, The Netherlands

The electrochemical nitrogen reduction reaction (NRR) is a promising alternative to the current greenhouse gas emission intensive process to produce ammonia (NH_3) from nitrogen (N_2). However, finding an electrocatalyst that promotes NRR over the competing hydrogen evolution reaction (HER) has proven to be difficult. This difficulty could potentially be addressed by accelerating the electrocatalyst development for NRR by orders of magnitude using high-throughput (HTP) workflows. In this work, we developed a HTP gas diffusion electrode (GDE) cell to screen up to 16 electrocatalysts in parallel. The key innovation of the cell is the use of expanded Polytetrafluoroethylene (ePTFE) gas diffusion layers (GDL) which simplifies the handling of catalyst arrays compared to carbon fabrics and enables sufficient N_2 mass transport. We demonstrate the robustness of the HTP workflow by screening 528 bimetallic catalysts of composition AB (A,B = Ag, Al, Au, Co, Cu, Fe, Mn, Mo, Ni, Pd, Re, Ru, W) for NRR activity. None of the materials produced ammonia significantly over background level which emphasizes the difficulty of finding active electrocatalysts for NRR and narrows down the search space for future studies.
 [DOI: 10.1149/1945-7111/aca6a7]

Manuscript submitted September 6, 2022; revised manuscript received November 12, 2022. Published December 8, 2022.

Supplementary material for this article is available online

The unequal distribution of renewable energy generation potential across the globe has created an awareness that a scalable means of storing and transporting electricity is needed to decarbonize the global economy. Green ammonia (NH_3), i.e., ammonia produced from renewable electricity has the potential to fill this gap, with additional potential to decarbonize ammonia production (1%–1.4% of global CO_2 emissions). One of the potentially cheapest routes to produce green NH_3 is the conversion of nitrogen (N_2) to NH_3 via the electrochemical nitrogen reduction reaction (NRR).[1–3] However, it has proven to be very challenging to find a selective catalyst that sufficiently suppresses the more favorable hydrogen evolution reaction (HER) in aqueous electrolyte such that high NH_3 production rates can be achieved. [4]

The difficulty of finding a selective catalyst for NRR is commonly attributed to the slow kinetics of the activation of the N_2 triple bond and the subsequent reduction in a 6-electron process compared to only 2-electron transfers for HER.[4] It is generally believed that the binding energies of key intermediates of the NRR mechanism are correlated (so-called scaling relations) which leads to a minimum overpotential requirement of 0.5 V for NRR according to density functional theory (DFT) calculations.[5] To overcome these difficulties, strategies are needed to promote NRR while simultaneously suppressing HER.

Alloying two or more metals can effectively tune the selectivity of electrochemical reactions. For example, Cu has been alloyed with Ag and Al to tune the selectivity of the CO_2 reduction reaction (CO2RR) towards ethanol or ethylene, respectively.[6,7] The improved electrocatalytic performance of alloys is often ascribed to strain, ligand and ensemble effects that create active sites with more optimal binding energies for key intermediates.[8–10] Possibly, an intermetallic catalyst exists that has a sufficient concentration of optimal active sites for NRR to promote the reaction and reach sufficient rates to prevail over HER.

Many recent studies claim that intermetallic materials such as Pd_3Cu_1, PdRu and AuCu are active catalysts for NRR.[11–14] However, several critical assessments of the NRR literature have concluded that the methodology that has been used thus far to assess the NRR activity of materials is unable to guarantee reliable results, because the performed control experiments were insufficient to exclude the possibility of a false positives from NH_3 and/or nitrogen oxides (NO_x) contamination.[15–17] This conclusion has led to a lack of confidence in published NRR results among NRR researchers which further intensified in view of the recent retractions and refutations of papers which were believed to be groundbreaking.[18,19]

To improve the reliability of NRR research, many control experiments to eliminate contamination sources and reduce the risk of false positives have been proposed.[15–17] In addition, we have recently argued that the choice of cell design has a large influence on the reliability of NRR experiments. By using gas diffusion electrode (GDE) cells instead of commonly used H-cells, the reliability of NRR experiments can be improved because experiments can be run at lower gas flow rates without limiting the N_2 mass transport to the catalyst surface, which in turn reduces the cost of crucial control experiments with $^{15}N_2$ (≈ €500/L).[20] The widespread adoption of reliable experimental protocols should restore the trust in published NRR results. Nevertheless, even with reliable protocols in place, two issues still slow down the progress of the research field. First, testing materials for NRR activity produces a lot of negative results which are much less likely to be published due to the bias of published literature to report preferably positive results.[21] Therefore new research cannot benefit from the knowledge of previous failed attempts. Second, the experimental workflow to test materials for NRR activity is too slow. With a median electrolysis time of 2 h per NRR experiment (cleaning steps and control experiments not included) catalyst testing is not fast enough for a thorough exploration of more complex material classes such as intermetallic catalysts.[20]

A promising strategy to accelerate the NRR experimental workflow is the implementation of parallelization and automation techniques. So-called high throughput (HTP) workflows are a powerful tool in heterogeneous catalysis.[22] For example the triply promoted iron catalyst that is currently used in the industrial production of ammonia was discovered by means of a HTP screening.[23] A HTP workflow for NRR catalyst development would not only drastically increase the likelihood of finding a promising catalyst but also produce large datasets to improve potentially invaluable computational models.[7] Such datasets would also include

[z]E-mail: m.kolen@tudelft.nl; f.m.mulder@tudelft.nl

a large number of negative results which could inform future research. In short, HTP workflows have the potential to enable more rapid advancements in the NRR research field.

To build a HTP workflow for NRR catalyst development, it is necessary to accelerate every step of the workflow. If one step is much slower than the others it will create a bottleneck and the overall acceleration will be small. Since HTP is a widely used method in other research fields, mature HTP methods for the production and physical characterization of catalyst libraries, and data analysis are available.[24] The key challenge seems to be the development of an electrochemical cell that is capable of rapidly screening materials for the target reaction. Common HTP cell designs to screen electrocatalysts are: single compartment cells with a composition spread as working electrode (WE) or WE array,[25–27] scanning capillary/probe/droplet cells,[28–30] arrays of single compartment cells[31] and membrane electrode assemblies (MEA).[32,33] Thus far, papers utilizing HTP workflows make up a negligible fraction of the published electrocatalysis literature which indicates that the available electrochemical cells have not yet reached sufficient technological maturity to replace one-by-one catalyst testing. Common problems with HTP cell designs include insufficient data quality compared to one-by-one catalyst testing,[34] short lifetime of cell components like current collectors[25] and catalysts adhesion issues.[26] Clearly, choosing an appropriate cell design is key for a meaningful HTP screening of NRR catalysts.

In all of the previously mentioned HTP cell designs (except MEA) the reactant gas is transported to the catalyst surface from the bulk electrolyte. Due to the low water solubility of N_2 (705.8 μM at 1 bar, 20 °C), the maximum rate of N_2 that can be transported to the catalyst surface in such cells corresponds to an NRR current density of only a few hundred μA cm^{-2}.[20,35] Screening catalysts under such N_2 limited conditions would lead to NRR selectivity losses which makes such cell designs unsuitable for an NRR catalyst screening.[36] MEA cell designs have sufficient N_2 mass transport but they use carbon fabric gas diffusion layers (GDL) as catalyst supports. Our attempts to work with carbon fabrics in a HTP cell failed due to practical issues. The main problem was that each catalyst required a separate carbon fabric to prevent short circuits between them during electrochemical tests. Each of these fabrics had to be cut out, transported, installed and electrically connected which proved to be a very time-consuming and error-prone process. In addition, carbon fabrics are very fragile with caused them to break frequently during handling. Therefore, we decided to explore other cell designs which have not been used in combination with HTP thus far to find a more convenient way of screening electrocatalysts.

Gas diffusion electrode cells have recently gained popularity as a platform to screen electrocatalysts in both the oxygen reduction reaction (ORR) and the CO2RR research field, because they allow testing of electrocatalysts under more realistic reaction conditions than conventional cell designs.[37–39] In GDE cells, the catalyst is positioned on a hydrophobic GDL at the junction between gas phase and liquid electrolyte. This close proximity of the catalyst surface to the gas phase enables high mass transport limiting currents for reactions which have gaseous reagents with low water solubility like N_2.[37,40] The simplicity of GDE cells in combination with their high N_2 transport and the previously discussed advantages for ammonia detection make GDE cells a preferable cell design for a HTP screening of NRR catalysts.[20,38] However, in most GDE cell experiments carbon fabric are used as the GDL which would cause the same limitations that were described above.[37,40] To enable the use of a GDE cell design for HTP screenings, these limitations must be overcome.

Recently, *Dinh* et al. showed that similar CO2RR performance to carbon fabrics can be obtained using a different type of GDL—expanded Polytetrafluoroethylene (ePTFE).[39] Interestingly, ePTFE is not electrically conductive which means that current can only flow through the catalyst layer deposited onto the ePTFE but not through the ePTFE itself. Thus, one piece of ePTFE can support a whole array of electrically insulated catalysts whereas one piece of carbon fabric can only support one catalyst. This not only drastically reduces the complexity of handling catalyst arrays but it also simplifies the electrical connection of catalysts in the electrochemical cell, because each catalyst is located at a well-defined position with respect to its neighbors. Additionally, ePTFE is less fragile than carbon fabrics and it becomes leak-tight under compression which reduces the complexity of a HTP cell even further. These advantageous properties of ePTFE may enable the development of a new generation of HTP cells with much simpler cell design and sufficient N_2 mass transport for NRR. Such cells have the potential to enable a drastic acceleration of the experimental throughput of NRR research compared to one-by-one catalyst testing.

In this work, we propose a HTP workflow to screen electrocatalysts for NRR and apply it to a screening of bimetallic catalysts. We first introduce a HTP method to produce bimetallic catalysts with well-defined compositions. We then describe the GDE cell design which utilizes ePTFE as GDL and characterize important characteristics of the cell such as reproducibility and N_2 mass transport. Next, we demonstrate that catalyst arrays can be physically characterized with methods that are compatible with a HTP workflow. Then, we use the workflow to screen 528 bimetallic catalysts for NRR activity in the temperature range 21 °C–55 °C. The catalyst screening was optimized for maximum throughput at the expense of resolution to maximize the chance of finding a promising catalyst for NRR.[22] Lastly, we evaluate the speed and robustness of the presented workflow by contrasting it with one-by-one catalyst testing.

Experimental

Preparation of bimetallic catalyst libraries.—16 bimetallic catalysts of varying composition were co-sputtered onto ePTFE (200 nm pore size, Pieper Filter GmbH) using a magnetron sputtering system (AJA International Inc.) equipped with 4 sputter guns (Figs. 1a, 1b). The sputter targets (purity: 99.9%-99.99%) were purchased from MaTecK. The base pressure of the sputtering chamber was 2e-7 mbar. Before a deposition, samples were sputter-cleaned under argon plasma for 2 min. Then, the sputter guns were turned on with closed shutter for 30 s. After that, the shutters were opened until the deposition was completed. Depositions were carried out under argon flow (flow rate: 20 sccm, purity: 99.9999%) at a pressure of 3 μbar. To control the composition of the co-sputtered composition gradients, the position-dependent deposition rate was measured for each metal by sputtering a thickness gradient on a microscope slide at a sputter gun power of 100 W (Fig. 1c). The thickness gradients were measured using a Dektak profilometer (Veeco). The catalyst arrays for the electrochemical tests were co-sputtered so that the catalyst layer thickness and composition in the center of the catalyst array were 300 nm and 50:50, respectively. The deposition time and the power of both sputtering guns to achieve this composition and thickness in the center of the catalyst array were calculated based on the deposition rates that were measured for each single metal using a Matlab script. For the calculations, it was assumed that the deposition rate of each metal is proportional to the deposition time and power setting of the sputter gun.[41] During the deposition of the catalyst arrays for the electrochemical tests, the sputter guns were positioned either at an angle of 90° or 180° with respect to each other (Fig. 1b). Henceforth, catalyst arrays that were sputtered at 90°/180° angle will be referred to as "90°-samples" and "180°-samples," respectively. An example of a 90°-sample and a 180°-sample is shown in Fig. 1d. The predicted composition on the ePTFE sample ranged from 20% ± 10% metal A on one side to 80% ± 10% metal A on the other side (Fig. 1e). The part of the ePTFE surface that was not supposed to be coated with metal was covered with a stainless steel mask (0.2 mm thickness). While we focussed on bimetallic catalysts in this work, many more classes of materials with potentially interesting properties for electrocatalysis can be produced by sputtering, for example high-entropy alloys, metal oxides and metal nitrides.[42,43]

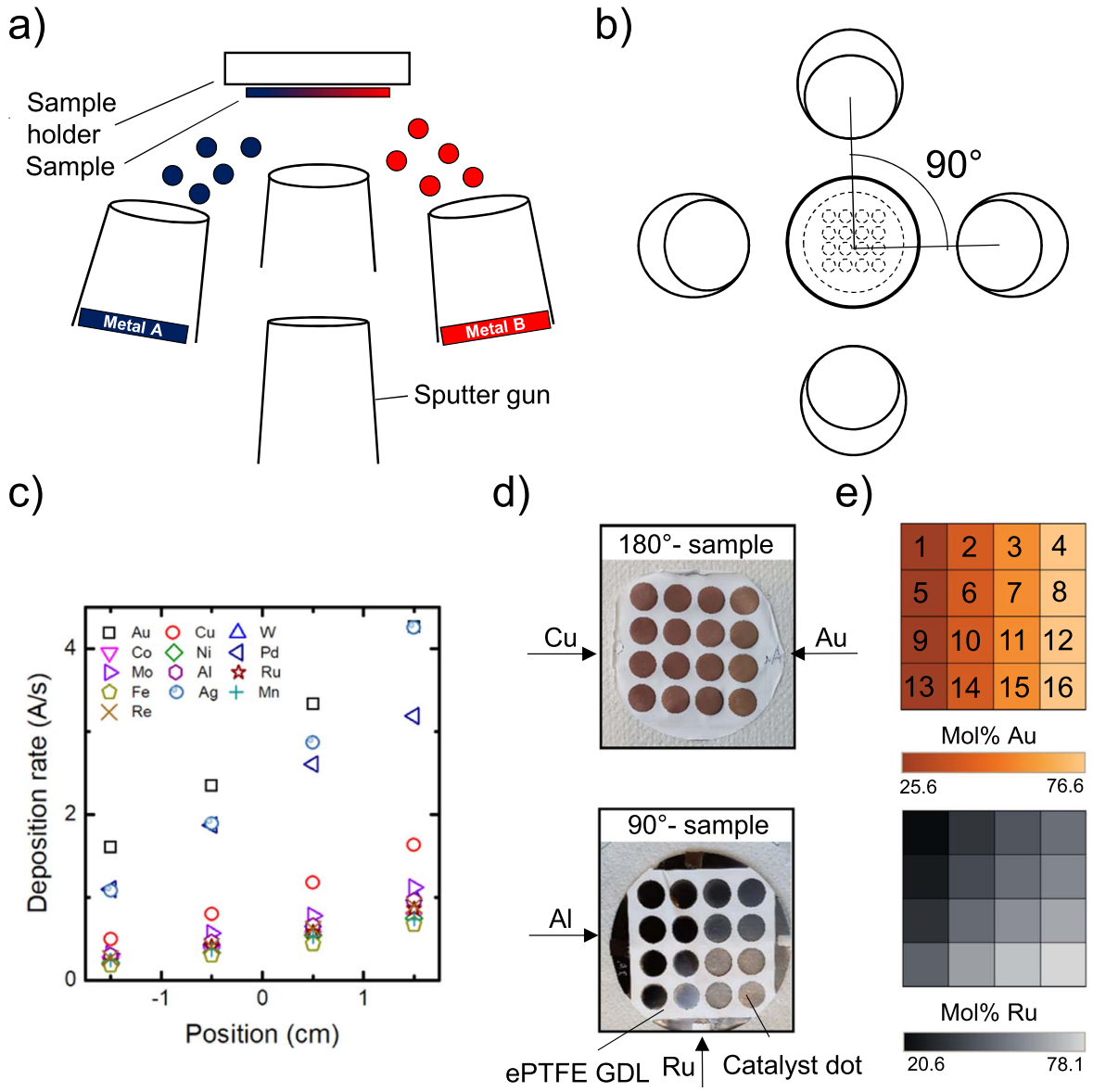

Figure 1. Sputtering setup used to deposit the catalyst arrays. (a) side view. (b) top view. (c) Deposition rate of each metal used in this work as a function of position. Position "0" corresponds to the center of the sample. (d) Example of a sample sputtered at 90°/180°. (e) Predicted composition map of the samples in (d).

To minimize the number of times the sputtering chamber had to be opened, all 4 metals in the chamber were co-sputtered with each other resulting in 6 unique bimetallic catalyst arrays (henceforth referred to as a set). The catalyst arrays that were screened for NRR activity in this work are listed in Table I. In total, 33 unique bimetallic catalyst arrays comprising 528 catalysts were screened. The choice of metals to be combined with each other was influenced by several factors. Practical constraints like the price and availability of sputtering targets, the compatibility of elements with the sputtering process and the need to minimize the number of sputter target changes were considered. The metals in set 1 were chosen based on literature reports claiming that Pd_3Cu_1, PdRu and AuCu are active catalysts for NRR.[11,12,14] For sets 2, 3 and 5, we predominantly choose metals that are active for heterogeneous ammonia synthesis (Fe, Ru, Co, Ni, Mn, Mo) to test if they are active for NRR, too.[23] To choose the metals in set 4, 7629 adsorption energies of nitrogen on bimetallic surfaces were downloaded from the Catalysis-Hub—a public database that contains the results of DFT calculations.[44] According to *Skúlason* et al., the most promising materials for NRR have a nitrogen adsorption energy in the range −0.5–0 eV.[45] Therefore, the materials with the most entries in this range were chosen for set 4. For set 6, we decided to combine the only element on the left side of the NRR volcano plot—Rhenium—with metals on the right side of the volcano because the resulting bimetallic catalysts might be closer to the peak of the volcano.[46]

Table I. Catalyst arrays that were screened for NRR activity in this work.

Set	Catalysts Arrays
1	CuAu, CuPd, CuRu, AuPd, AuRu, PdRu
2	FeCu, FeNi, FeW, CuNi, CuW, NiW
3	PdCo, PdMo, PdNi, CoMo, CoNi, MoNi
4	CoAl, CoRu, CoFe, AlRu, AlFe, RuFe
5	NiCu, NiAg, NiMn, CuAg, CuMn, AgMn
6	ReCu, ReFe, RePd, CuFe, CuPd, FePd

Setup for HTP catalyst screening.—A schematic of the setup that was used to screen the electrocatalyst arrays for NRR activity is

shown in Fig. 2a. The cell was constructed like a 3-compartment GDE cell but instead of one, an array of 16 WEs was positioned at the interface between the gas compartment and catholyte. The electrolyte reaches the catalyst layer but cannot penetrate the ePTFE due to the hydrophobicity of the material (Fig. 2b). The abrupt interface between electrolyte and gas ensures high N_2 mass transport to the catalyst surface.[39] All catalysts are in contact with the same catholyte which means that the ammonia production can only be measured for a whole catalyst array at a time, not for individual catalysts. We chose this configuration because inactive catalysts can be filtered out with minimal NH_3 detection effort. A Celgard 3401 membrane was used as a separator between the catholyte and anolyte. A Mini Hydroflex reversible hydrogen electrode (Gaskatel GmbH) and a nickel foil (thickness: 0.0125 mm, purity: 99.9%, supplier: GoodFellow) were used as reference electrode (RE) and counter electrode (CE), respectively. All electrochemical tests were done using an RT-2000 multichannel potentiostat with 24 independent floating channels (Arbin Instruments) and a Parstat MC potentiostat (Ametek). To electrically connect each of the 16 catalysts to the multichannel potentiostat, a printed circuit board (PCB) was custom-designed and manufactured by JLCPCB. The PCB was sandwiched between the gas compartment and the catholyte compartment of the HTP cell to create an electrical contact between the catalysts and the current collectors on the PCB (Fig. 2b). The current collectors on the PCB are electrically connected to pin header connectors which enables quick connection of the multichannel potentiostat to all 16 catalysts (Fig. 2c). Each hole in the PCB has a diameter of 6 mm which exposes a catalyst surface area of 0.28 cm^2 to the electrolyte. To prevent contamination of the electrolyte with substances from the PCB, a silicone coating (RS-components) was applied to the PCB. The catholyte and anolyte were recirculated between cell and reservoirs using a Masterflex L/S peristaltic pump. A Bronkhorst mass flow controller (MFC) and mass flow meter (MFM) were installed to control the flow of N_2 into the cell and measure the flow of N_2 leaving the cell, respectively. The temperature of the system was controlled using a home-built oven. Downstream of the gas compartment, a gas chromatography-mass spectrometry (GC-MS) measured the concentration of NH_3, O_2 and H_2 in the gas phase. The details of the GC-MS method have been presented elsewhere.[47] A home-built liquid trap was installed

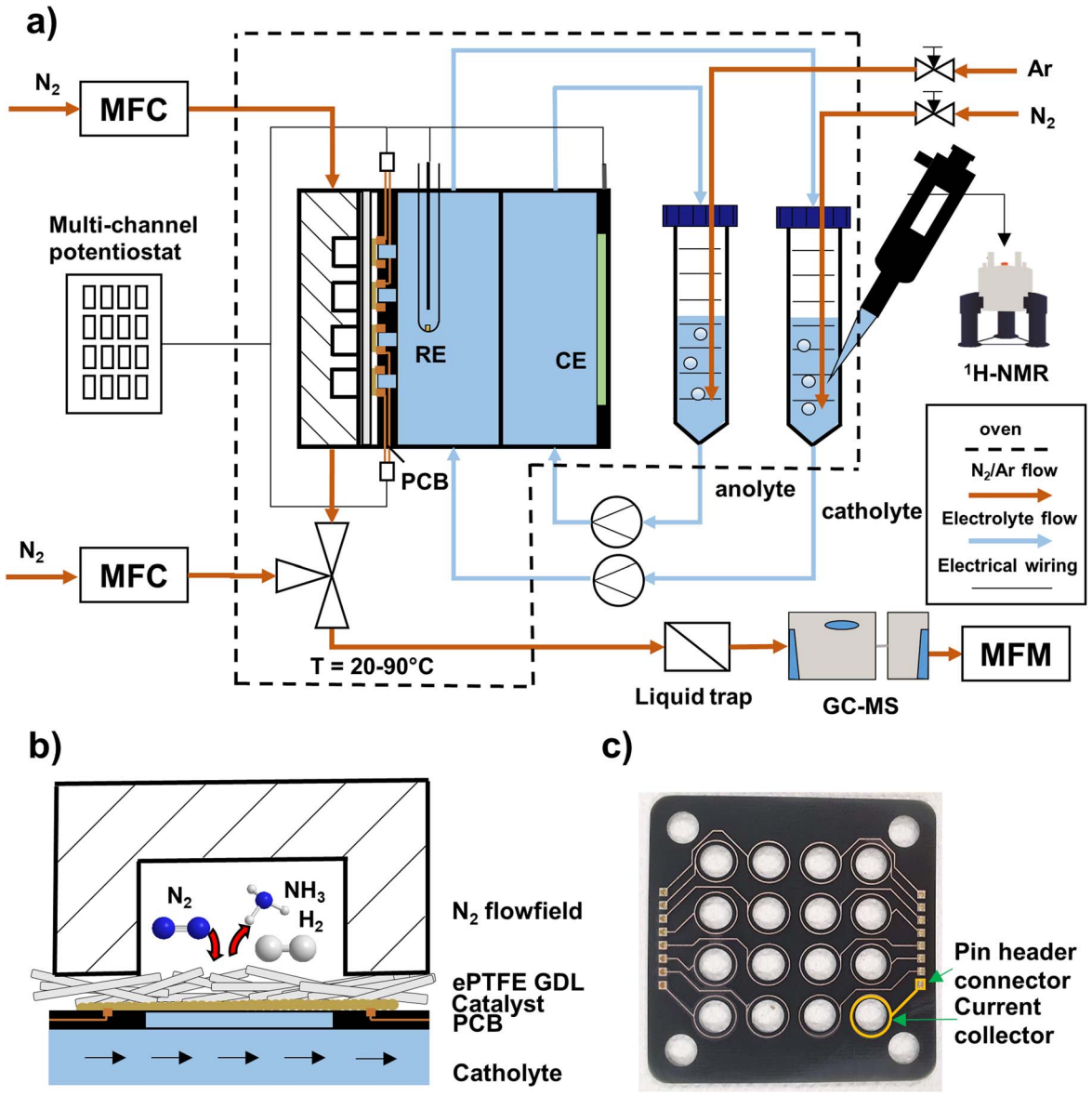

Figure 2. (a) Schematic of the experimental setup to screen 16 bimetallic electrocatalysts in parallel in a gas diffusion electrode cell. (b) Zoomed-in schematic of one catalyst to illustrate how each catalyst was supplied with electrons, N_2 and electrolyte. (c) Photograph of the printed circuit board (PCB) that was used to electrically connect the catalyst array to the potentiostat.

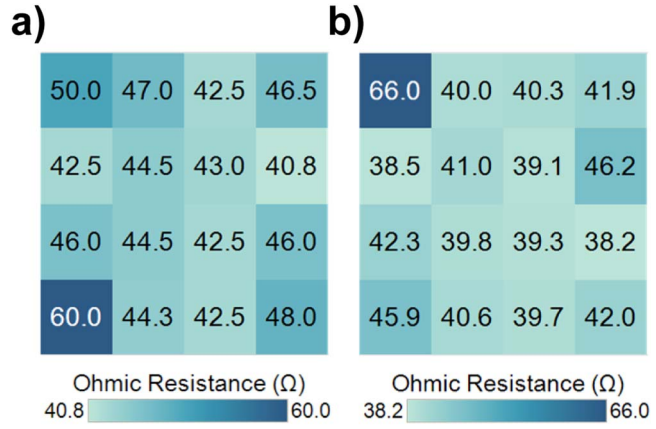

Figure 3. (a), (b) Ohmic resistance map for two separate samples containing 16 300 nm Ag catalysts.

as a precautionary measure to prevent flooding of the GC-MS with electrolyte. However, the liquid trap might be redundant, because electrolyte did not enter the gas compartment a single time during our experiments. N_2 and Ar were supplied by Linde and had a purity of 99.999%. N_2 and Ar were not purified because the concentration of NH_3 in both was below the detection limit of our GC (150 ppb) and the NO concentration in both was less than 10 ppb as measured with an NO analyzer (Teledyne 200E). Since we used low flow rates (1–10 sccm) and short electrolysis durations (<75 min), contaminations at this level are too low to cause false positives.[16] Additionally, we measured both the NH_3 and NO_x background in the electrolyte for every experiment with NMR and Ion Chromatography (IC), respectively and found no correlation between the background level and the amount of gas that was in contact with the electrolyte.

Electrochemical tests.—In a typical experiment, a catalyst array was first positioned over the electrical contacts of the PCB. After assembly of the cell, the catalyst array was checked for short-circuits using an ohmmeter. To minimize NH_3 and NO_x backgrounds, 0.1 M KOH (prepared fresh daily) was recirculated between cell and reservoirs 2–3 times for 5 min each. The flow rate of the catholyte and anolyte was set to 15 ml min^{-1} during all cleaning steps and electrochemical tests. For the electrochemical test, the reservoirs of catholyte and anolyte were filled with 14 ml and 12 ml 0.1 M KOH, respectively. The O_2 in the electrolyte was removed by bubbling N_2 or Ar into the catholyte and anolyte for at least 15 min while recirculating the electrolyte. The flow rate of N_2 and Ar into the reservoirs was set to approximately 10 sccm using a needle valve. The gas compartment of the cell was flushed with N_2 at a flow rate of 10 sccm. To equilibrate any processes that might take place on the catalyst surface once a current is applied (reconstruction, dissolution), a preelectrolysis step was carried out before the electrochemical characterization. During the preelectrolysis step, the same current that would later be applied during the catalyst screening was applied to each catalyst for 5 min. The electrochemical characterization of the attainable currents and voltages was carried out by applying a chronopotentiometry (CP) staircase in the current density range 1.4–4.3 mA cm^{-2} consisting of 5 steps of 30 s each. Only one catalyst at a time was characterized this way. Since the electrochemical characterization of all 16 catalysts of every catalyst array would have been too time-consuming, only the catalysts at positions 1,6,11,16 and 14,15,16,17 were characterized for a 90°/180°-sample, respectively (catalyst position according to Fig. 1e). Prior to the electrolysis step to measure the NRR activity of the catalysts, the flow rate of the gas bubbling into the electrolyte reservoirs was reduced to approximately 3 sccm to minimize potential NH_3/NO_x contaminations from the feed gas. The N_2 flow rate into the gas compartment was set to 1 sccm unless high oxygen levels made it necessary to increase the flow rate to prevent ORR on the catalyst surfaces. Two CP steps were carried out to measure the NRR activity of the catalyst arrays. During both CP steps a constant current was applied to all catalysts in parallel. The first CP step was carried out at room temperature (henceforth referred to as "RT-experiment") and had a duration of 70 min. The current density that was applied to each catalyst ranged from 1–10 mA cm^{-2} and depended on its position in the cell and the orientation of the sputter guns during co-sputtering of the sample (90° or 180°). A map that shows which current density was applied to each catalyst position for a 90°/180°-sample is shown in Fig. S1. In general, we tried to minimize redundancy and test as many different current densities and catalyst layer thicknesses for each composition as possible. During the second CP step (henceforth referred to as "55 °C-experiment), the same current densities as during the RT-experiment were applied for 60 min while the electrolyte was slowly heated to 55 °C using a custom build oven. The heating profile of the oven (Fig. S2) allowed a GC-MS injection every 5 °C–10 °C. Water condensation in the gas line had to be prevented to avoid damage to the GC-MS. Therefore, the gas stream exiting the cell was diluted with N_2. The dilution was gradually increased with increasing temperature of the electrolyte from 1:2.5 in the beginning to 1:10 after 30 min. After an experiment, the cell was disassembled and the catalyst array was removed from the PCB. Residues of the previous catalyst were removed from the PCB with grade 1200 abrasive sheets (RS-components). Before reusing, the PCB was washed with soap and rinsed with Milli-Q water. To quantify NH_3/NO_x backgrounds a 2 ml sample was taken from the catholyte after the O_2 removal step. The ammonia production during the RT-experiment and the 55 °C-experiment was determined by taking a 1 ml sample from the catholyte after each step.

iR-compensation.—The uncompensated ohmic resistance between the RE and a catalyst was found to depend on the position of the catalyst in the cell. Figures 3a and 3b show a map of the ohmic resistance between the 16 WEs and the RE as a function of their respective position in the cell for two catalyst arrays consisting of 16 Ag catalysts with identical Ag layer thickness (300 nm), measured by electrochemical impedance spectroscopy (EIS). The maximum resistance deviation was 16 Ω which would only cause a 9.6 mV shift in potential at the current of electrochemical characterizations (600 μA). This potential inaccuracy is negligible for the scope of our screening which is focused on finding selective catalysts. Therefore, we used the resistance map in Fig. 3a to compensate iR-drops during all electrochemical characterizations (100% post-correction). No iR-compensation was possible for experiments with multiple catalysts running in parallel because during those experiments the electric field of up to 16 WEs overlapped each other which would have made iR-compensation very complex.

Results and Discussion

Physical characterisation.—To demonstrate that HTP characterization with XRD can be integrated into the workflow, we measured the XRD patterns of a 180°-PdRu-sample (Fig. 4) and a 90°-PdAu-sample (Fig. S3). The diffraction peaks at 2θ = 38.3°, 42.2°, 44°, 58.3°, 69.4° and 78.4° of the 180°-PdRu-sample could be assigned to the characteristic (100), (002), (101), (102), (110), (103) crystal planes of the Ru reference pattern, respectively and the diffraction peaks at 2θ = 40.1°, 46.7°, 68.1° could be assigned to the characteristic (111), (200), (220) crystal planes of the Pd reference pattern, respectively. Since the catalysts were sputtered at 180°, catalysts in the same column have a similar composition (Fig. 1e) which leads to similar XRD patterns (Fig. 4a). A shift from a Pd-rich (catalysts 1 to 4) to a Ru-rich composition (catalysts 13 to 16) can be observed which agrees well with the expected shift in composition for a 180°-PdRu-sample. The diffraction peaks of the 90°-PdAu-sample are shifted with respect to the reference patterns of Pd and Au which shows that alloys were formed. To examine the morphology of ePTFE with and without catalysts deposited onto

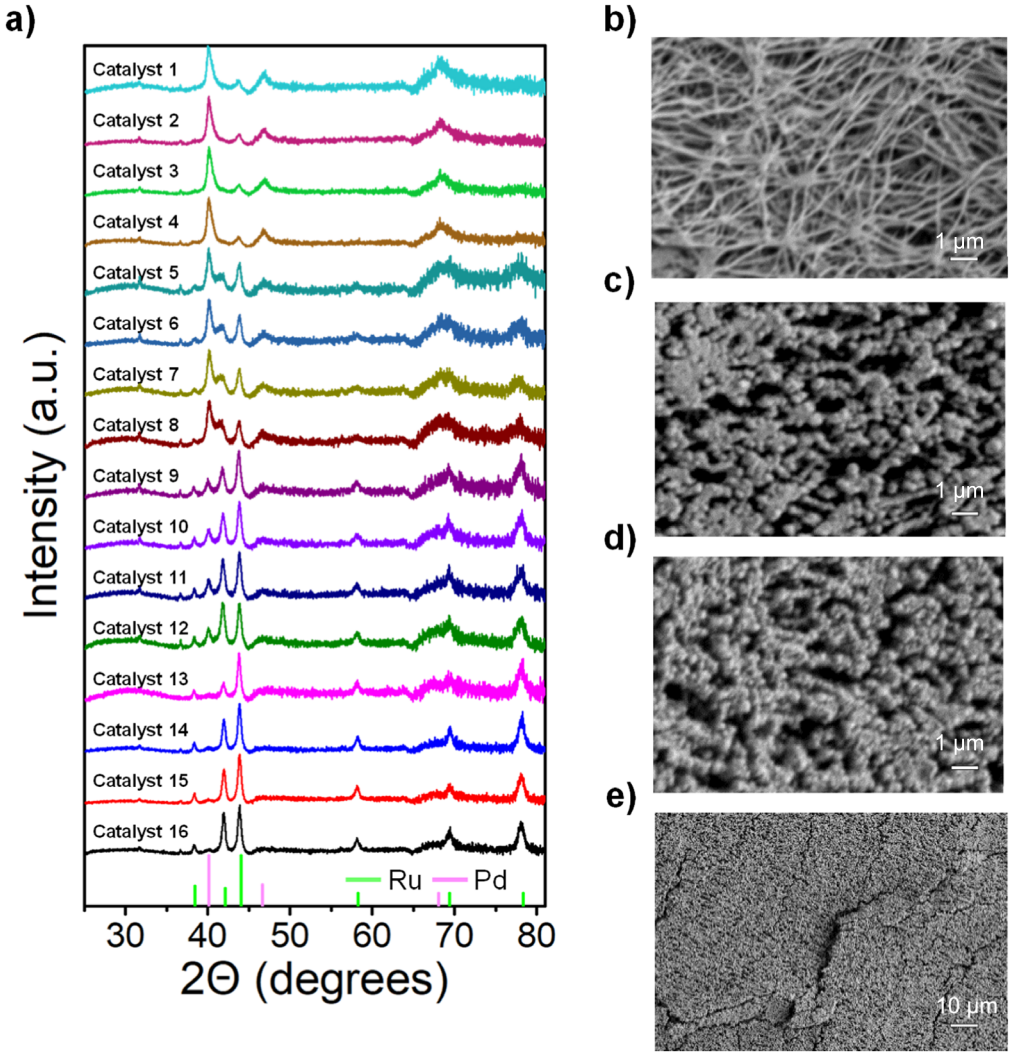

Figure 4. (a) XRD patterns of a PdRu catalyst array sputtered at 180° and reference patters of Ru and Pd. (b) SEM image of ePTFE with 200 nm pore size. (c), (d) SEM images of 300 nm PdCu sputtered on ePTFE before and after electrolysis, respectively. (e) Same position as (d) but with lower magnification. Acceleration voltage for SEM images: 5 kV.

it, we recorded SEM images of a PdCu sample (Figs. 4b–4e). Figure 4b shows the morphology of the ePTFE before deposition. The material is comprised of macroscopically-small Teflon filaments which form a fibrous network. After deposition of 300 nm PdCu, the surface was almost completely covered with PdCu (Fig. 4c). After the electrochemical experiments to measure the NRR activity the morphology seems similar at high magnification but at lower magnification cracks in the surface are visible (Figs. 4d, 4e).

Control of thin-film composition.—To validate that the composition of material libraries produced for this study can be accurately controlled using co-sputtering, we sputtered a CoMo composition gradient onto a microscope slide and measured its bulk composition using EDX (Fig. 5a). The measured composition gradient agrees well with the predicted compositions from the deposition rates of Co and Mo. This confirms that the bulk compositions of catalyst arrays can be accurately controlled by co-sputtering. To measure if the surface composition of CoMo also agrees well with predicted values, the surface compositions of a 180°-sample of CoMo was measured with XPS and compared against the predicted compositions (Figs. 5b, 5c). The surface compositions of CoMo agree well with the predicted compositions for the top two catalyst rows whereas a shift towards higher than predicted Co mole fractions can be observed for the bottom two rows. After the electrochemical tests to measure NRR activity, the surface of most catalysts is strongly enriched in Co which indicates that Mo either dissolved into the electrolyte or was replaced by Co on the surface (Fig. 5d). Interestingly, in the rows with the lowest initial Co concentration (bottom two) the Co composition increases from left to right after electrolysis which indicates that the applied current density during electrolysis might influence how much Mo remains on the surface. The applied current density during the electrochemical tests was 10 mA cm^{-2} on the left side and decreases stepwise to 1 mA cm^{-2} on the right side which indicates that high applied current densities might stabilize Mo on the surface if the initial Co concentration is less than 50 mol%. A detailed investigation of the phenomena underlying these composition changes goes beyond the scope of this work. What is important to know for this study is that initial bulk compositions of catalysts can be accurately controlled but surface compositions, especially after contact with the electrolyte, might differ strongly from the initial bulk composition. While being able to control initial bulk compositions is sufficient for a preliminary catalyst screening (which is the goal of this study), studies that aim to measure activity-composition relationships must use in situ/operando tools to measure the surface composition during electrolysis.

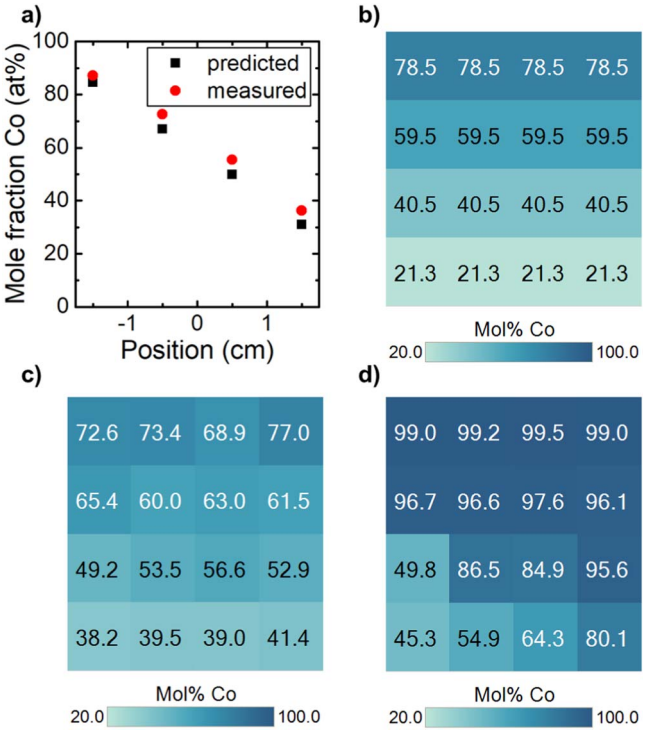

Figure 5. (a) Comparison of the composition of a CoMo thin film (co-sputtered on a microscope slide) predicted from the sputter rates of Co, Mo and the bulk composition measured by EDX. (b) Predicted composition of a 180°-CoMo-sample from the sputter rates of Co, Mo (c),(d) measured surface composition by XPS before and after electrolysis, respectively.

Characterization of the N_2 mass transport.—An important prerequisite for any HTP catalyst screening is that false negatives (i.e. non-discovery of active materials although they were part of the screened library) must be prevented.[22] In the following, we will discuss some of the control experiments that were carried out to confirm that some common causes of false negatives can be excluded in this study. For the sake of brevity, we will only discuss the N_2 mass transport and the reproducibility of electrochemical characterizations in the main manuscript. Further control experiments to confirm that no side reactions occurred and that the ammonia detection worked properly for every sample can be found in the SI.

To confirm that NRR selectivity losses due to N_2 mass transport limitations can be avoided with the HTP GDE cell, we wanted to measure the mass transport limiting current for NRR. However, the mass transport limiting current for NRR cannot be measured directly because there is no selective catalyst for this reaction, yet. Instead, we used ORR to characterize the mass transport which should give comparable results because O_2 and N_2 have similar water solubility.[35,48] Figure 6a shows the polarization curve of a 300 nm Ag catalyst measured in N_2 and in a gas mixture of 5.2% O_2 in N_2. In 5.2% O_2, the onset of ORR begins around 0.8 V vs reversible hydrogen electrode (RHE) and reaches a plateau around 0.1 V vs RHE. In N_2, HER starts at around −0.4 V vs RHE which is sufficiently far away from the start of the ORR plateau in 5.2% O_2 to ensure that HER did not contribute significantly to the ORR limiting current measured in 5.2% O_2. To measure the ORR mass transport limited current density in 5.2% O_2 for each catalyst position in the cell, we subsequently applied a potential of 0 V vs RHE to all 16 Ag catalysts for 150 s (Fig. 6b). As Fig. 6c shows, the stable current after 150 s is 10–22 mA cm^{-2} for three fresh Ag samples. As Fig. 6d shows, the O_2 mass transport depends linearly on the O_2 concentration which means that the current density measured in 5.2% O_2 can be extrapolated to 100% O_2. The resulting mass transport limited current density in 100% O_2 is 192–423 mA cm^{-2}. For comparison, other HTP cells such as single compartment cells or scanning droplet cells reach ORR mass transport limitations at two orders of magnitude lower current densities (around 0.6–1.6 mA cm^{-2}).[25,30,34] Therefore, NRR selectivity losses due to mass transport limitations can be prevented with the HTP GDE cell.

Reproducibility of the electrochemical characterization.—We investigated the reproducibility of electrochemical characterizations with the HTP cell by measuring linear scan voltammetry (LSV) scans for a catalyst array consisting of 300 nm Ag catalysts. As demonstrated in Fig. 7, the reproducibility across the different catalysts of the array is very good (only around 50 mV maximum potential difference). The potential difference may be caused by morphological inhomogeneities across the ePTFE. GDEs with small geometric surface area are especially prone to these deviations because manufacturing inhomogeneities across the GDE cannot be averaged out as for larger samples.[38] To test the reproducibility of the electrochemical characterization across different samples we repeated the test with a Ag catalyst array produced under identical conditions and found that the LSV's from the second sample closely matches those from the first sample. One LSV from a catalyst of the second sample slightly deviates from the other LSVs at higher current density. The potential difference increases linearly with the current density which indicates that this catalyst has a higher ohmic resistance than the other catalysts. Presumably, the increase in resistance was caused by a reduced electrical contact between the PCB and the catalyst. The potential difference between the catalyst with higher resistance and the rest was around 50 mV at the current which was used for electrochemical characterizations (600 μA) in the following. Therefore, the electrochemical characterization is very reproducible across different catalysts of an array and different samples but in rare cases increases in resistance can lead to potential shifts up to 50 mV.

Characterization of the electrochemical HER activity.—Since HER is the main competing reaction of NRR, a comprehensive dataset of the HER activity of bimetallic catalysts may be useful for the selection of promising catalysts for NRR. However, no such dataset is publicly available, yet. Therefore, we show in Fig. 8 the electrode potential of 4 compositions from each bimetallic catalyst array at a current density of 2.14 mA cm^{-2} (i.e. 600 μA current). We chose a current density of only 2.14 mA cm^{-2} to minimize errors from uncompensated ohmic resistance between the RE and the catalyst array.

Each bimetallic catalyst appears twice in Fig. 8, both as AB and BA which makes it easier to compare all bimetallic catalysts containing a certain metal. The HER activity was highest ($E > -200$ mV) for most Ni- and Pd-catalysts and lowest ($E < -400$ mV) for transition metal oxides (W-, Mn-catalysts). This activity trend agrees well with the expected activity of these metals from literature data.[49–51] Similarly, the activity trend of different Ni-catalysts agrees well with literature.[52,53] A more detailed comparison of HER activity trends with literature is available in the SI. Due to the difficulty of producing NH_3 concentrations above background level from NRR (see the following section), we were unable to predict promising materials for NRR from the HER activity data. However, the data might benefit future efforts in this direction.

NRR activity of bimetallic electrocatalysts.—To quantify the NRR activity of each catalyst array, we measured the difference between the NH_3 concentration in the electrolyte before and after every experiment (henceforth referred to as "NH_3 production") and calculated the corresponding NRR current. Since all 16 catalysts of an array were placed in the same electrolyte, it was only possible to measure the combined NRR current of a catalyst array and not the individual NRR current density of each catalyst. The NRR current of all catalyst arrays is shown in Fig. 9 and Fig. 10 for the RT-experiment and the 55 °C-experiment, respectively. Besides the color gradient to visualize the NRR current we also reported the NH_3

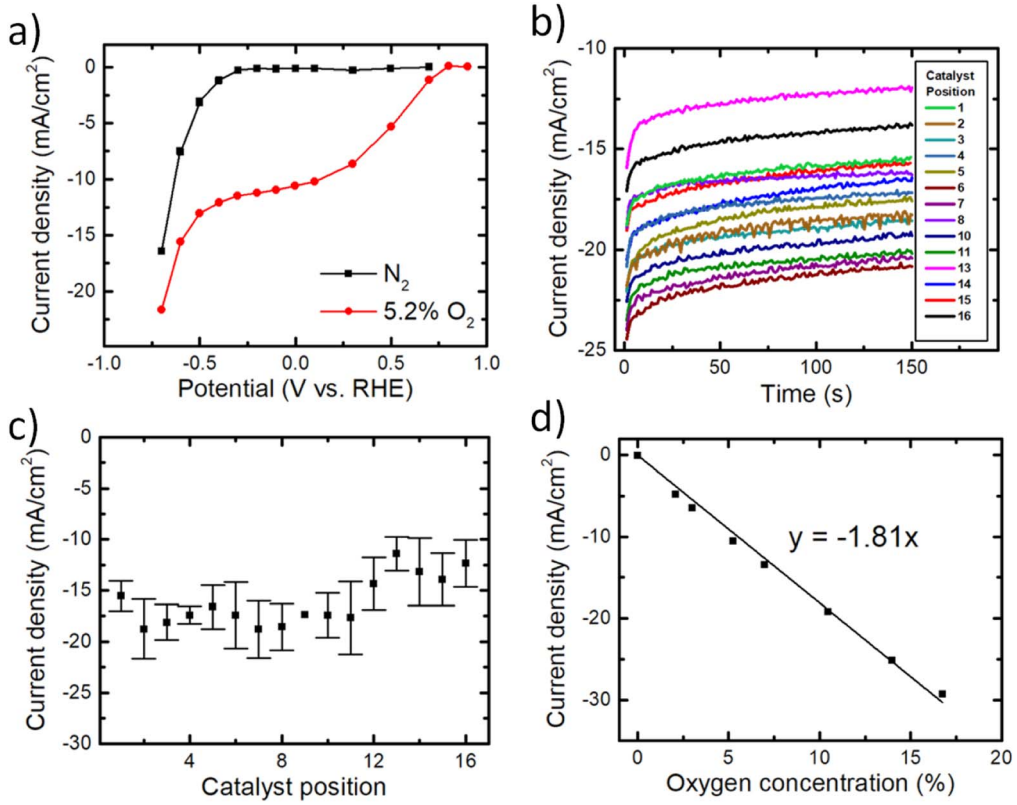

Figure 6. (a) Polarization curve of a 300 nm Ag catalyst measured in pure N_2 and 5.2% O_2 in N_2. (b) Chronoamperometry at 0 V vs RHE for 150 s in 5.2% O_2 for 16 300 nm Ag catalysts. (c) Average current density during the last 5 s of the experiment in (b). Error bars represent a triplet measurement with different samples. (d) Dependence of current density at 0 V vs RHE on the oxygen concentration entering the gas compartment of the cell. The data is not iR-compensated.

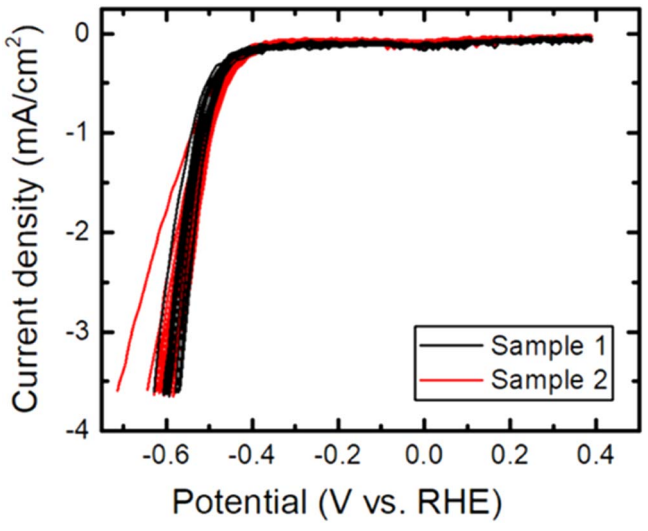

Figure 7. Reproducibility of LSVs measured for two catalyst arrays consisting of 300 nm Ag catalysts. Scan rate: 15 mV s^{-1}.

production underlying the calculation of the NRR current and the NH_3/NO_x background for all catalyst arrays. Negative NRR currents (blue) in Fig. 9 and Fig. 10 were most likely caused by larger NH_3 backgrounds in the liquid sample taken before the electrochemical experiment was started. No data from the gaseous NH_3 detection is shown because the detection limit of the GC-MS (1 ppm NH_3 in the gas phase) was not reached by any catalyst array.

The largest NRR current that we measured was around 9 μA (CoMo during the 55 °C-experiment). Even if all of the 9 μA NRR current were produced by only one of the 16 catalysts of a catalyst array, this corresponds to an NRR current density of ≈30 μA cm^{-2} (electrode area: 0.28 cm^2) which is only around 10% faradaic efficiency (FE) at the lowest current density used during the screening. Therefore, the most important result of this work is that the 528 bimetallic catalysts that were screened in this work are not promising catalysts for NRR under the tested conditions. If any of the screened catalysts were active for NRR at all their faradaic efficiency was less than 10%.

It is apparent from Fig. 9 and Fig. 10 that NH_3/NO_x backgrounds between 0–4 μM were present for every tested catalyst array. At such low concentrations, there are many different potential contamination sources. Some of those contamination sources such as the atmosphere, human breath or surfaces that are in contact with the electrolyte are difficult to remove which leads to unavoidable backgrounds. Other research groups have reported unavoidable backgrounds on the order of 0.5–2 μM during their NRR experiments which agrees well with our observations.[17,54,55] It is very easy to misinterpret NH_3/NO_x backgrounds as NRR activity because some contamination sources can cause a linear increase of the NH_3 concentration over time (e.g. NO_x electroreduction to NH_3 or a slow leaching process from a membrane), which looks like NRR activity.[20] To avoid being misled by false positives, we only carried out further experiments with a catalyst array if its NH_3 production was significantly higher than the common NH_3 background. The threshold for further investigation was 3-fold the common NH_3/NO_x background of 4 μM (i.e. 12 μM). Unfortunately, the NH_3 production of all catalyst arrays in Fig. 9 and Fig. 10 was below this threshold which means that the NH_3 production from NRR (if present if all) of all tested catalyst arrays was indistinguishable from NH_3 contamination.

As a side note, it is noteworthy that both the NH_3 and NO_x background had considerable variance over time which suggests that it is insufficient to measure either one of these backgrounds only during one experiment and assume they remain constant for all

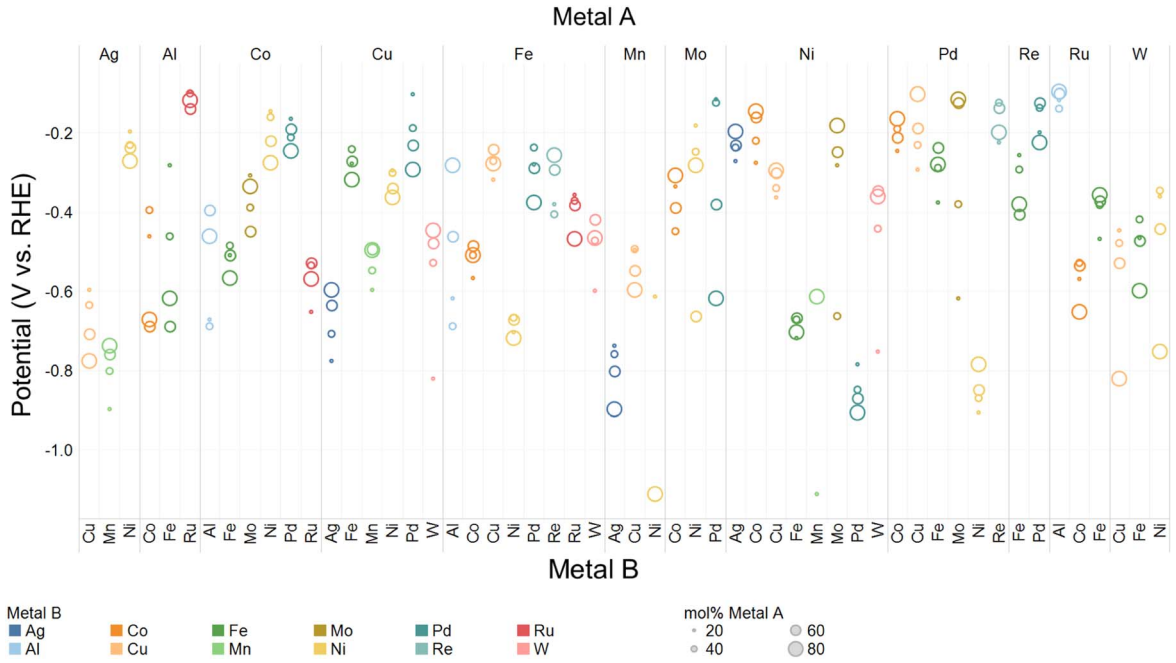

Figure 8. Average potential during the last 5 s of the electrochemical characterization at 0.6 mA (2.14 mA cm^{-2}) for each catalyst tested in this work. The size of the symbols represents the predicted mole fraction of metal A in the catalyst (accuracy: ±10%). Some data points of MnNi are outside of the plotted range. Each composition appears twice, both as AB and BA.

following experiments as it is frequently done in the NRR research field to prove that no contaminations were present during experiments.[16] Instead, NH_3/NO_x backgrounds must be measured and reported for every NRR experiment, especially if NRR activity is deduced from NH_3 productions on the order of a few μM. In addition, we believe that the NRR research field would benefit from more transparently reported backgrounds because, as we have shown above, the magnitude of backgrounds relative to alleged NH_3 production from NRR is a great indicator for the reliability of measurements.

We observed spikes in the NH_3 production for NiCu (16.6 μM) at room temperature and for FeCu (17 μM) and PdCu (71 μM) during the 55 °C-experiment. However, subsequent attempts to reproduce these results failed which means that the original results were caused by NH_3 contamination. Random spikes of the NH_3 concentration in the electrolyte are common in NRR research. For example gloves, sample storage containers or cell surfaces can randomly introduce large amounts of NH_3 which can lead to false conclusions.[17,55] In the case of PdCu, the NH_3 contamination might have originated from the reduction of NO_x, because an unusually high NO_x background (35.9 μM) was measured before the electrolysis was started. This is plausible because Cu is known to be an efficient catalyst for NO_x reduction to NH_3.[56] To avoid misleading the reader, we don't report these false positives in Fig. 9 and Fig. 10.

The NH_3 production of some catalyst arrays was slightly higher than the common NH_3 background of 4 μM. In some cases (e.g. CuW, RuPd at room temperature), this coincided with the presence of an elevated NH_3/NO_x background indicating the experiment might have been more contaminated than the rest. In other cases (e.g. CuMn, CuPd, FePd at room temperature), we did not measure an elevated NH_3/NO_x background which would explain the slightly elevated NH_3 production. While these cases could simply be spikes in NH_3 contamination introduced after the background sample was taken, the NH_3 might also have originated from N-impurities in the catalyst layer. Yu et al. showed that μM-levels of NH_3 in the electrolyte might originate from nitrogen impurities which were incorporated into sputtered CoMo thin films during the sputtering process.[57] Since CoMo had the highest NH_3 production of all catalysts during the 55 °C-experiment we suspect that nitrogen impurities incorporated during the sputtering process might have contributed to the slightly elevated NH_3 productions of some catalyst arrays. However, a systematic investigation of NH_3 contaminations from the sputtering process goes beyond the scope of this work.

Since none of the tested bimetallic catalysts produced NH_3 significantly above background level, it is questionable if bimetallic catalysts are promising for future NRR catalyst development efforts. This view is supported by theoretical considerations based on DFT calculations by *Montoya* et al. who argued that alloying is not a promising strategy for NRR catalyst development because alloying is unlikely to break the scaling relations between key adsorbates of the NRR mechanism.[5] However, we have only screened a small fraction of the bimetallic composition space. It is therefore possible that active bimetallic catalysts were missed in this work. In addition, the selectivity of electrocatalytic reactions can be influenced by many factors (e.g. electrolyte, pressure, catalyst morphology etc.) which were not varied in this study. Therefore, bimetallic catalysts which were inactive for NRR in our study might be active under different conditions.[58] Our large dataset of negative results is counteracting the overrepresentation of positive results in literature.[21] Until published positive results of NRR activity meet the requirements of unambiguous NH_3 detection, large datasets of negative results might be more useful to steer future research towards the most promising catalyst development strategies.[15–17]

Screening speed and robustness with the HTP GDE cell.—The primary goal of developing a HTP catalyst screening workflow is to increase the speed of a catalyst screening. Therefore, we want to briefly analyze how much quicker catalysts can be screened with the workflow presented in this work and which steps must be accelerated for further improvements. With the HTP workflow presented in this work it took approximately 40 h to screen one set (i.e. 96 catalysts) which is approximately an order of magnitude faster than traditional approaches. Assuming no downtime in a highly automated system, approximately 5000 catalysts could be screened per year at this speed. It took between 6–16 h to sputter the catalyst arrays. The duration of the sputtering step depended strongly on how many sputter rates had to be measured before the sputtering of the catalyst arrays. The characterization steps using XRD and XPS took only

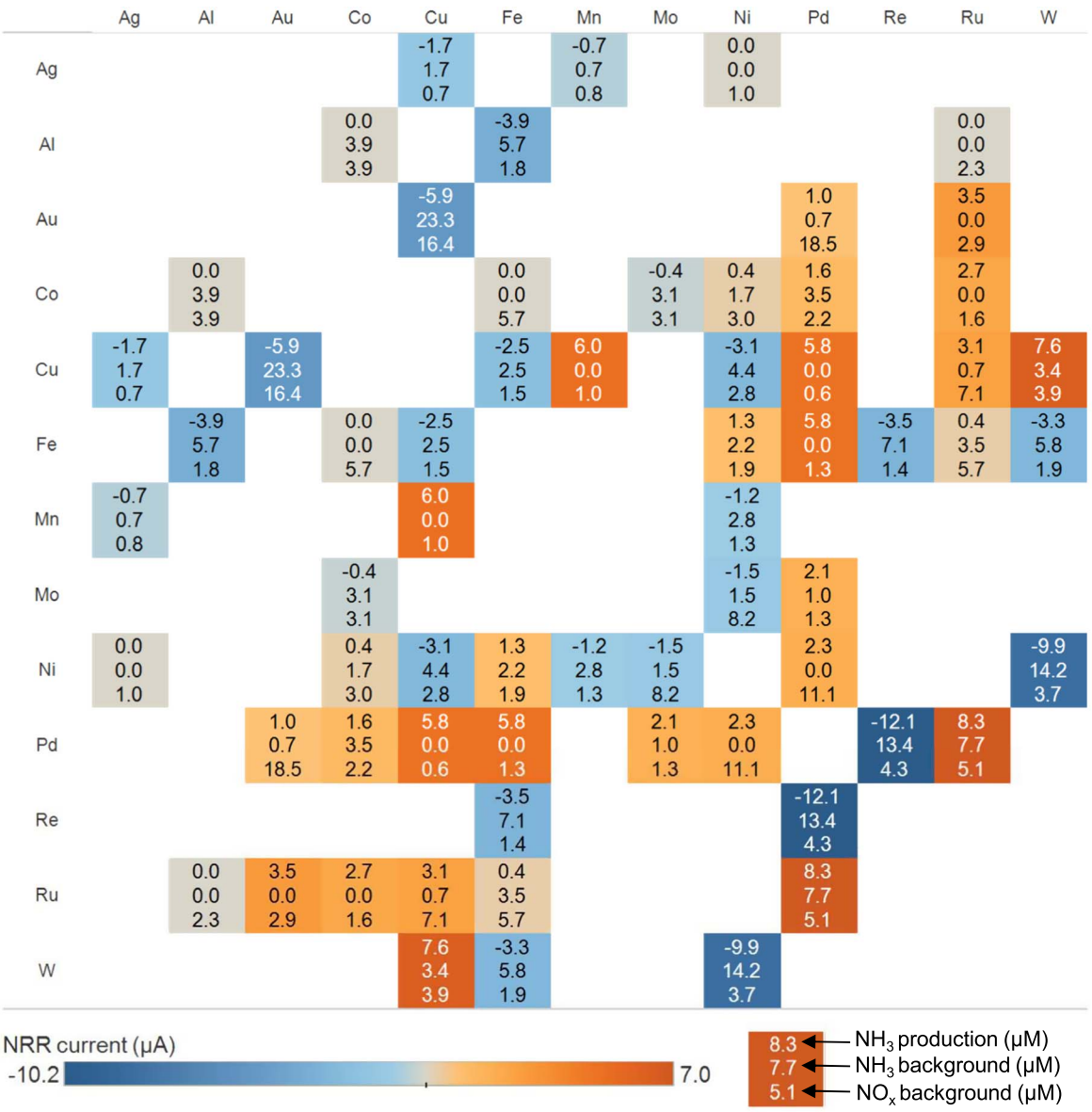

Figure 9. NRR activity of the bimetallic catalysts during the RT-experiment. The color represents the NRR current that corresponds to the NH_3 production assuming that all NH_3 was produced from NRR. The NH_3 production, NH_3 background and NO_x background are reported for each catalyst array.

around 2 h of bench time per catalyst set because the machines were mostly automated and could run overnight. However, the data processing and analysis of the physical characterization data proved to be a bottleneck which is why we only did this for selected catalyst arrays. The electrochemical experiments to screen one set took around 24 h (including all preparation steps) and the product analysis step took an additional 2–3 h (including data analysis and visualization). Therefore, the most time-consuming steps are the electrochemical experiments and the catalyst deposition which should be the focus of future acceleration efforts. An electrical contact between catalyst and multichannel potentiostat was successfully established for 97% of the screened catalysts which confirms that the robustness of the cell is comparable to cells used for one-by-one catalyst testing (see SI for more information).

Conclusions

We presented a high-throughput workflow to screen bimetallic electrocatalysts for NRR activity which is approximately an order of magnitude faster than a one-by-one catalyst screening and can be adapted to other reactions of interest and other classes of materials. The close proximity of a gas phase to the catalyst surface in the GDE cell design used for the catalyst screening enables two orders of magnitude higher mass transport limiting currents for reactions with gaseous reactants such as N_2 or O_2 which circumvents selectivity losses due to mass transport limitations. A screening of 528 bimetallic catalysts for NRR activity did not yield an active catalyst for the reaction. In the absence of unambiguous positive results, large datasets of negative results for NRR, as the one we presented in this work, might be the best available option to steer future research in the direction of the most promising catalyst development strategies.

Acknowledgments

This work is part of the Direct Electrolytic Ammonia Production project with project number 15234, which is financed by The Netherlands Organisation for Scientific Research (NWO). The authors would like to thank Xiaohui Liu for her help with XRD measurements.

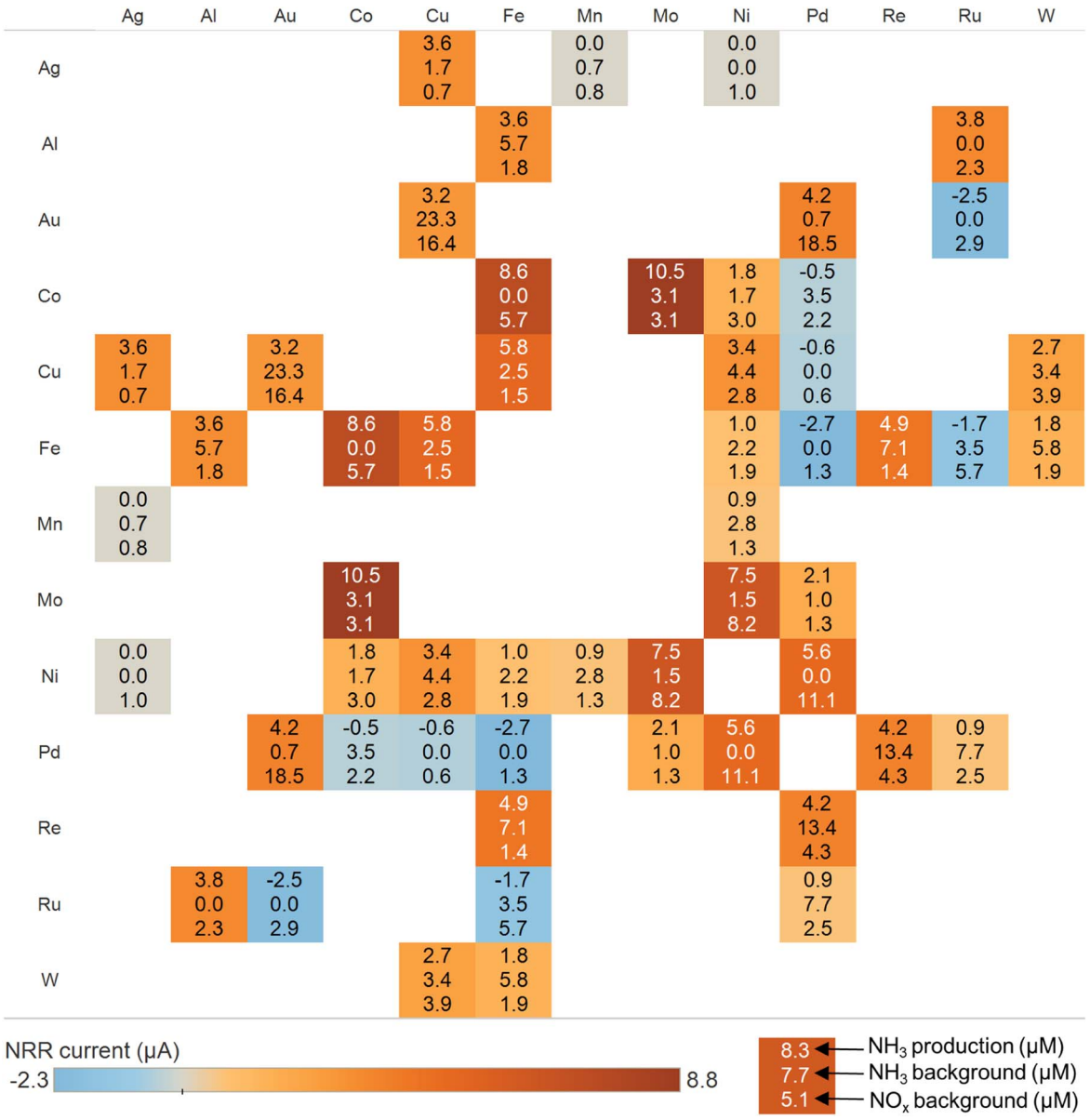

Figure 10. NRR activity of the bimetallic catalysts during the 55 °C-experiment. The color represents the NRR current that corresponds to the NH_3 production assuming that all NH_3 was produced from NRR. The NH_3 production, NH_3 background and NO_x background are reported for each catalyst array.

Supporting Information

The following files are available free of charge.

Experimental details, NH_3/NO_x detection details, discussion of HER activity measurements, calculations, results of cell validation experiments, photographs of catalyst arrays, plots of the potential during RT-experiments and 55 °C-experiments (Word file).

ORCID

Martin Kolen https://orcid.org/0000-0002-6309-4521
Herman Schreuders https://orcid.org/0000-0002-7993-2489
Bart Boshuizen https://orcid.org/0000-0002-3413-8839
Dylan D. van Noordenne https://orcid.org/0000-0002-6713-6936
Davide Ripepi https://orcid.org/0000-0001-7488-6690
Wilson A. Smith https://orcid.org/0000-0001-7757-5281
Fokko M. Mulder https://orcid.org/0000-0003-0526-7081

References

1. D. R. MacFarlane, P. V. Cherepanov, J. Choi, B. H. R. Suryanto, R. Y. Hodgetts, J. M. Bakker, F. M. Ferrero Vallana, and A. N. Simonov, "A roadmap to the ammonia economy." *Joule*, **4**, 1186 (2020).
2. A. Valera-Medina, H. Xiao, M. Owen-Jones, W. I. F. David, and P. J. Bowen, "Ammonia for power." *Prog. Energy Combust. Sci.*, **69**, 63 (2018).
3. F. M. Mulder, "Implications of diurnal and seasonal variations in renewable energy generation for large scale energy storage." *J. Renewable Sustainable Energy*, **6**, 033105 (2014).
4. A. R. Singh, B. A. Rohr, J. A. Schwalbe, M. Cargnello, K. Chan, T. F. Jaramillo, I. Chorkendorff, and J. K. Nørskov, "Electrochemical ammonia synthesis—the selectivity challenge." *ACS Catal.*, **7**, 706 (2017).
5. J. H. Montoya, C. Tsai, A. Vojvodic, and J. K. Nørskov, "The challenge of electrochemical ammonia synthesis: a new perspective on the role of nitrogen scaling relations." *ChemSusChem*, **8**, 2180 (2015).
6. Y. C. Li et al., "Binding site diversity promotes CO_2 electroreduction to ethanol." *J. Am. Chem. Soc.*, **141**, 8584 (2019).
7. M. Zhong et al., "Accelerated discovery of CO_2 electrocatalysts using active machine learning." *Nature*, **581**, 178 (2020).

8. I. E. L. Stephens, A. S. Bondarenko, U. Grønbjerg, J. Rossmeisl, and I. Chorkendorff, "Understanding the electrocatalysis of oxygen reduction on platinum and its alloys." *Energy Environ. Sci.*, **5**, 6744 (2012).
9. J. A. Rodriguez, "Physical and chemical properties of bimetallic surfaces." *Surf. Sci. Rep.*, **24**, 223 (1996).
10. V. Ponec, "Alloy catalysts: the concepts." *Appl. Catal., A*, **222**, 31 (2001).
11. Z. Wang, C. Li, K. Deng, Y. Xu, H. Xue, X. Li, L. Wang, and H. Wang, "Ambient nitrogen reduction to ammonia electrocatalyzed by bimetallic pdru porous nanostructures." *ACS Sustainable Chem. Eng.*, **7**, 2400 (2019).
12. F. Pang, Z. Wang, K. Zhang, J. He, W. Zhang, C. Guo, and Y. Ding, "Bimodal nanoporous Pd_3Cu1 alloy with restrained hydrogen evolution for stable and high yield electrochemical nitrogen reduction." *Nano Energy*, **58**, 834 (2019).
13. W. Tong, B. Huang, P. Wang, L. Li, Q. Shao, and X. Huang, "Crystal-phase-engineered PdCu electrocatalyst for enhanced ammonia synthesis." *Angew. Chem. Int. Ed.*, **59**, 2649 (2020).
14. Y. Liu, L. Huang, X. Zhu, Y. Fang, and S. Dong, "Coupling Cu with Au for enhanced electrocatalytic activity of nitrogen reduction reaction." *Nanoscale*, **12**, 1811 (2020).
15. L. F. Greenlee, J. N. Renner, and S. L. Foster, "The use of controls for consistent and accurate measurements of electrocatalytic ammonia synthesis from dinitrogen." *ACS Catal.*, **8**, 7820 (2018).
16. J. Choi, B. H. R. Suryanto, D. Wang, H.-L. Du, R. Y. Hodgetts, F. M. Ferrero Vallana, D. R. MacFarlane, and A. N. Simonov, "Identification and elimination of false positives in electrochemical nitrogen reduction studies." *Nat. Commun.*, **11**, 5546 (2020).
17. S. Z. Andersen et al., "A rigorous electrochemical ammonia synthesis protocol with quantitative isotope measurements." *Nature*, **570**, 504 (2019).
18. J. Choi, H.-L. Du, C. K. Nguyen, B. H. R. Suryanto, A. N. Simonov, and D. R. MacFarlane, "Electroreduction of nitrates, nitrites, and gaseous nitrogen oxides: a potential source of ammonia in dinitrogen reduction studies." *ACS Energy Lett.*, **5**, 2095 (2020).
19. S. Licht, B. Cui, B. Wang, F.-F. Li, J. Lau, and S. Liu, "Retraction." *Science*, **369**, 780 (2020).
20. M. Kolen, D. Ripepi, W. A. Smith, T. Burdyny, Mulder, and M. Fokko, "Overcoming nitrogen reduction to ammonia detection challenges: the case for leapfrogging to gas diffusion electrode platforms." *ACS Catal.*, **12**, 5726 (2022).
21. S. L. Scott, T. B. Gunnoe, P. Fornasiero, and C. M. Crudden, "To Err is human; to reproduce takes time." *ACS Catal.*, **12**, 3644 (2022).
22. A. Hagemeyer, P. Strasser, and A. F. Volpe, *In High-Throughput Screening in Chemical Catalysis* (New York, Wiley) 1 (2004).
23. H. Liu, *In Ammonia synthesis catalysts: innovation and practice* (Singapore)(World Scientific)32 (2013).
24. T. H. Muster, A. Trinchi, T. A. Markley, D. Lau, P. Martin, A. Bradbury, A. Bendavid, and S. Dligatch, "A review of high throughput and combinatorial electrochemistry." *Electrochim. Acta*, **56**, 9679 (2011).
25. J. F. Whitacre, T. I. Valdez, and S. R. Narayanan, "A high-throughput study of PtNiZr catalysts for application in PEM fuel cells." *Electrochim. Acta*, **53**, 3680 (2008).
26. M. Prochaska, J. Jin, D. Rochefort, L. Zhuang, F. J. DiSalvo, H. D. Abruña, and R. B. van Dover, "High throughput screening of electrocatalysts for fuel cell applications." *Rev. Sci. Instrum.*, **77**, 054104 (2006).
27. J. S. Cooper and P. J. McGinn, "Combinatorial screening of fuel cell cathode catalyst compositions." *Appl. Surf. Sci.*, **254**, 662 (2007).
28. J. A. Haber, C. Xiang, D. Guevarra, S. Jung, J. Jin, and J. M. Gregoire, "High-throughput mapping of the electrochemical properties of (Ni-Fe-Co-Ce)O_x oxygen-evolution catalysts." *ChemElectroChem*, **1**, 524 (2014).
29. J. M. Gregoire, C. Xiang, X. Liu, M. Marcin, and J. Jin, "Scanning droplet cell for high throughput electrochemical and photoelectrochemical measurements." *Rev. Sci. Instrum.*, **84**, 024102 (2013).
30. J.-P. Grote, A. R. Zeradjanin, S. Cherevko, A. Savan, B. Breitbach, A. Ludwig, and K. J. J. Mayrhofer, "Screening of material libraries for electrochemical CO_2 reduction catalysts—improving selectivity of Cu by mixing with Co." *J. Catal.*, **343**, 248 (2016).
31. K. C. Neyerlin, G. Bugosh, R. Forgie, Z. Liu, and P. Strasser, "Combinatorial study of high-surface-area binary and ternary electrocatalysts for the oxygen evolution reaction." *J. Electrochem. Soc.*, **156**, B363 (2009).
32. R. Liu and E. S. Smotkin, "Array membrane electrode assemblies for high throughput screening of direct methanol fuel cell anode catalysts." *J. Electroanal. Chem.*, **535**, 49 (2002).
33. D. A. Stevens, J. M. Rouleau, R. E. Mar, A. Bonakdarpour, R. T. Atanasoski, A. K. Schmoeckel, M. K. Debe, and J. R. Dahn, "Characterization and PEMFC testing of Pt[Sub 1−x]M[Sub x] (M = Ru,Mo,Co,Ta,Au,Sn) anode electrocatalyst composition spreads." *J. Electrochem. Soc.*, **154**, B566 (2007).
34. A. K. Schuppert, A. A. Topalov, I. Katsounaros, S. O. Klemm, and K. J. J. Mayrhofer, "A scanning flow cell system for fully automated screening of electrocatalyst materials." *J. Electrochem. Soc.*, **159**, F670 (2012).
35. R. Battino, T. R. Rettich, and T. Tominaga, "The solubility of nitrogen and air in liquids." *J. Phys. Chem. Ref. Data*, **13**, 563 (1984).
36. J. Newman and K. E. Thomas-Alyea, *In Electrochemical Systems* (New York, Wiley-Interscience) 491 (2004).
37. J. Schröder, V. A. Mints, A. Bornet, E. Berner, M. Fathi Tovini, J. Quinson, G. K. H. Wiberg, F. Bizzotto, H. A. El-Sayed, and M. Arenz, "The gas diffusion electrode setup as straightforward testing device for proton exchange membrane water electrolyzer catalysts." *JACS Au*, **1**, 247 (2021).
38. K. Ehelebe et al., "Benchmarking fuel cell electrocatalysts using gas diffusion electrodes: inter-lab comparison and best practices." *ACS Energy Lett.*, **7**, 816 (2022).
39. C.-T. Dinh et al., "CO_2 electroreduction to ethylene via hydroxide-mediated copper catalysis at an abrupt interface." *Sci.*, **360**, 783 (2018).
40. T. Burdyny and W. A. Smith, "CO_2 reduction on gas-diffusion electrodes and why catalytic performance must be assessed at commercially-relevant conditions." *Energy Environ. Sci.*, **12**, 1442 (2019).
41. A. H. Simon, "Sputter Processing." *In Handbook of Thin Film Deposition* (Amsterdam, Elsevier) 55 (2012).
42. L. Banko, O. A. Krysiak, J. K. Pedersen, B. Xiao, A. Savan, T. Löffler, S. Baha, J. Rossmeisl, W. Schuhmann, and A. Ludwig, "Unravelling composition–activity–stability trends in high entropy alloy electrocatalysts by using a data-guided combinatorial synthesis strategy and computational modeling." *Adv. Energy Mater.*, **12**, 2103312 (2022).
43. D. Ripepi, R. Zaffaroni, H. Schreuders, B. Boshuizen, and F. M. Mulder, "Ammonia synthesis at ambient conditions via electrochemical atomic hydrogen permeation." *ACS Energy Lett.*, **6**, 3817 (2021).
44. K. T. Winther, M. J. Hoffmann, J. R. Boes, O. Mamun, M. Bajdich, and T. Bligaard, "Catalysis-Hub.Org, an open electronic structure database for surface reactions." *Sci Data*, **6**, 75 (2019).
45. E. Skúlason, T. Bligaard, S. Gudmundsdóttir, F. Studt, J. Rossmeisl, F. Abild-Pedersen, T. Vegge, H. Jónsson, and J. K. Nørskov, "A theoretical evaluation of possible transition metal electro-catalysts for N_2 reduction." *Phys. Chem. Chem. Phys.*, **14**, 1235 (2012).
46. Z. W. Seh, J. Kibsgaard, C. F. Dickens, I. Chorkendorff, J. K. Nørskov, and T. F. Jaramillo, "Combining theory and experiment in electrocatalysis: insights into materials design." *Sci.*, **355**, eaad4998 (2017).
47. D. Ripepi, R. Zaffaroni, M. Kolen, J. Middelkoop, and F. M. Mulder, "*Operando* isotope selective ammonia quantification in nitrogen reduction studies via gas chromatography-mass spectrometry." *Sustain. Energy Fuels*, **6**, 1945 (2022).
48. G. A. Truesdale and A. L. Downing, "Solubility of oxygen in water." *Nature*, **173**, 1236 (1954).
49. Z. Chen, X. Duan, W. Wei, S. Wang, and B.-J. Ni, "Recent advances in transition metal-based electrocatalysts for alkaline hydrogen evolution." *J. Mater. Chem. A*, **7**, 14971 (2019).
50. F. Safizadeh, E. Ghali, and G. Houlachi, "Electrocatalysis developments for hydrogen evolution reaction in alkaline solutions—a review." *Int. J. Hydrogen Energy*, **40**, 256 (2015).
51. Y. Zhu, Q. Lin, Y. Zhong, H. A. Tahini, Z. Shao, and H. Wang, "Metal oxide-based materials as an emerging family of hydrogen evolution electrocatalysts." *Energy Environ. Sci.*, **13**, 3361 (2020).
52. I. A. Raj and K. I. Vasu, "Transition metal-based hydrogen electrodes in alkaline solution ? electrocatalysis on nickel based binary alloy coatings." *J. Appl. Electrochem.*, **20**, 32 (1990).
53. M. A. Domínguez-Crespo, M. Plata-Torres, A. M. Torres-Huerta, E. M. Arce-Estrada, and J. M. Hallen-López, "Kinetic study of hydrogen evolution reaction on Ni30 Mo70, Co30Mo70, Co30Ni70 and Co10Ni20Mo70 alloy electrodes." *Mater. Charact.*, **55**, 83 (2005).
54. R. Hodgetts, H.-L. Du, D. R. MacFarlane, and A. N. Simonov, "Electrochemically induced generation of extraneous nitrite and ammonia in organic electrolyte solutions during nitrogen reduction experiments." *ChemElectroChem*, **8**, 1596 (2021).
55. W. Yu, N. S. Lewis, H. B. Gray, and N. F. Dalleska, "Isotopically selective quantification by UPLC-MS of aqueous ammonia at submicromolar concentrations using dansyl chloride derivatization." *ACS Energy Lett.*, **5**, 1532 (2020).
56. B. H. Ko, B. Hasa, H. Shin, Y. Zhao, and F. Jiao, "Electrochemical reduction of gaseous nitrogen oxides on transition metals at ambient conditions." *J. Am. Chem. Soc.*, **144**, 1258 (2022).
57. W. Yu, P. Buabthong, C. G. Read, N. F. Dalleska, N. S. Lewis, H.-J. Lewerenz, H. B. Gray, and K. Brinkert, "Cathodic NH_4^+ leaching of nitrogen impurities in CoMo thin-film electrodes in aqueous acidic solutions." *Sustain. Energy & Fuels*, **4**, 5080 (2020).
58. S. Nitopi et al., "Progress and perspectives of electrochemical CO_2 reduction on copper in aqueous electrolyte." *Chem. Rev.*, **119**, 7610 (2019).